

Single-Site Metal-Organic Framework Catalysts for the Oxidative Coupling of Arenes via C-H/C-H activation

Niels Van Velthoven,^a Steve Waitschat,^b Sachin M. Chavan,^{cd} Pei Liu,^e Simon Smolders,^a Jannick Vercammen,^a Bart Bueken,^a Sara Bals,^e Karl Petter Lillerud,^{cd} Norbert Stock^{bd} and Dirk E. De Vos^{*a}

a: Centre for Surface Chemistry and Catalysis, KU Leuven, Celestijnenlaan 200F p. o. box 2461, 3001 Leuven (Belgium)

b: Institute of Inorganic Chemistry, Christian-Albrechts University Kiel, Max-Eyth-Straße 2, 24118 Kiel (Germany)

c: Department of Chemistry, University of Oslo, p. o. box 1033 Blindern, 0315 Oslo (Norway)

d: ProfMOF AS, Kirkegårdsveien 45, 3616 Kongsberg (Norway)

e: Electron Microscopy for Materials Science, University of Antwerp, Groenenborgerlaan 171, 2020 Antwerp (Belgium)

Contents

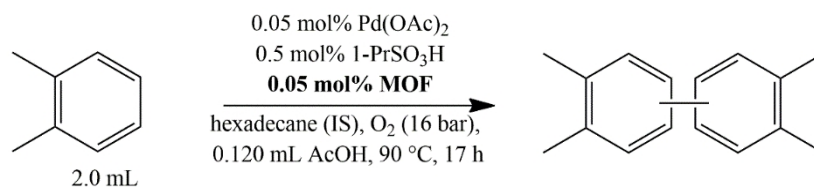
General information	2
General procedure catalytic reactions	2
MOF synthesis	3
MOF-808.....	3
UMCM-309a	4
Zr-abtc	4
UiO-66-COOH	5
UiO-66	5
UiO-67-bipy	5
Zirconium oxide.....	6
Smopex-102.....	6
MOF loading	6
Optimization of the reaction conditions	7
Palladium leaching.....	9
Hot filtration test.....	10
PXRD	10
Substrate scope.....	13
MOF stability	14
Product inhibition experiments.....	15
Catalyst reactivation.....	16
FTIR.....	17
EXAFS.....	18

High-angle annular dark-field scanning transmission electron microscopy (HAADF-STEM)	20
Influence of the oxygen pressure	22
Determination of the Kinetic Isotope Effect	22
References	23

General information

All commercially available compounds were used as received. Product quantification was performed on a Shimadzu GC-2010 with a DB-1ht column and a flame ionization detector, while an Agilent 6890 gas chromatograph with a HP-1 MS column and a 5973 MSD mass spectrometer was used for product identification. Liquid ^1H NMR spectra were recorded on a Bruker AMX-300 spectrometer at 300 MHz (16 scans) and the data were analyzed using the MestReNova 12.0.2 software package. Powder X-ray diffraction (PXRD) data were recorded on a Malvern PANalytical Empyrean diffractometer equipped with a PIXcel 3D 1x1 detector. Samples were loaded onto a 96-well sample holder and patterns were recorded at room temperature in transmission geometry within a $1.3^\circ - 50^\circ 2\theta$ -range with a step size of 0.013° . The theoretical patterns were simulated by Mercury 3.10 based on the corresponding CIF-files. The leached palladium content in solution was determined by ICP-OES using a Varian 720-ES after evaporating the organics and redissolving the metal residue in aqua regia. Fourier transform infrared spectroscopy (FTIR) was performed on a potassium bromide (FTIR grade, Sigma-Aldrich) pellet containing 10 wt % MOF using a Nicolet 6700 spectrometer. The pellet was activated *in situ* under vacuum (1 mbar) at 100°C for 2 h to remove physisorbed water. Pd K-edge X-ray absorption spectroscopy (XAS) spectra were collected at the DUBBLE XAFS beam line (BM26A) of the European Synchrotron Radiation Facility and analyzed with the Athena and Artemis software packages.^{1,2} Normalization of the data and background removal were performed in Athena and the X-ray absorption edge energy was calibrated using the spectrum of Pd^0 foil. Artemis and its integrated FEFF6 software were used for the extended X-ray absorption fine structure (EXAFS) analysis and the fits were made in R-space with the k^2 -weighted Fourier-transformed EXAFS data. High-angle annular dark-field scanning transmission electron microscopy (HAADF-STEM) images for energy-dispersive X-ray spectroscopy (EDX) were collected using an aberration corrected cubed FEI Titan microscope operating at an acceleration voltage of 300 kV. The samples were prepared by diluting the powder in ethyl acetate and depositing drops of the suspension on a copper grid covered with a holey carbon film.

General procedure catalytic reactions



Generally, 2.000 mL (16.58 mmol) *o*-xylene (99 %, Acros), 8.30 μL (82.85 μmol ; 0.5 mol %) 1-propanesulfonic acid (95 %, Acros), 0.118 mL (2.07 mmol; 12.5 mol %) acetic acid (glacial, Fisher) and 0.100 mL hexadecane (internal standard) (>99 %, Sigma-Aldrich) were added to 1.86 mg (8.29 μmol ; 0.05 mol %) Pd(OAc)_2 (99.9 %, Acros) and (8.29 μmol ; 0.05 mol %) MOF in a 10 mL stainless steel autoclave. The reactors were flushed three times with pure O_2 to remove the remaining air and subsequently pressurized with pure O_2 to 16 bar. The valves were then closed and the reactors were placed in a preheated 4-well aluminum block. The reaction was conducted under stirring at 90°C for 17 hours. After reaction, the reactors were cooled on ice, the MOF was separated from the reaction

medium via centrifugation and the products were analyzed using GC-FID/GC-MS. This procedure was also used to acquire the data of the reaction kinetics. In accordance to literature reports,^{3,4} the TON is defined as $\text{TON} = 2 \times \text{mole (biaryl)} / \text{mole (Pd)}$. **Note: a thorough safety assessment has to be made before applying such hazardous conditions and these reactions should only be performed in proper equipment that ensures safe handling at all times.**

MOF synthesis

MOF-808

MOF-808 was synthesized in a 250 mL Teflon lined stainless steel autoclave by dissolving 3.220 g (10.00 mmol) zirconyl chloride octahydrate (>98 %, Acros) and 0.700 g (3.33 mmol) trimesic acid (95 %, Sigma Aldrich) in 100 mL DMF (>99 %, Acros) and 56 mL acetic acid (glacial, Fisher). The resulting solution was then placed in a synthesis oven at 135 °C for 24 h.

After synthesis, the obtained precipitate was washed three times with DMF, three times with ethanol and dried at room temperature. In each step, the material was centrifuged at 4000 rpm for 20 min and the supernatant was decanted. After the first washing steps, 1.000 g MOF-808 was redispersed in 100 mL of a 0.1 M aqueous solution of sodium acetate (99 %, Acros) for 24 h under mild stirring to remove the chloride anions which can cap the Zr-clusters (*vide infra*). Afterwards, the material was washed three times with deionized water. In order to remove the acetate modulators from the Zr-clusters, an adapted literature procedure was followed.⁵ The 'wet' MOF-808 powder was first redispersed in 100 mL of a 0.1 M aqueous solution of 1-propanesulfonic acid (95 %, Acros). Finally, the material was washed three times with deionized water, three times with ethanol and dried at 115 °C under vacuum (1 mbar) for 24 hours. The removal of the acetate modulators was confirmed by ¹H NMR after digesting the samples in hydrofluoric acid.

Since the Zr-clusters of both MOF-808 and UMCM-309a are only 6-fold coordinated by the organic linkers, the remaining six coordination sites are occupied mostly by the modulator (acetate or formate) but also by chloride anions. These chloride anions can poison the active palladium catalyst, so removing the chloride anions by an extra washing step with a 0.1 M aqueous solution of sodium acetate is necessary to obtain high TONs in the first run (Figure S1).

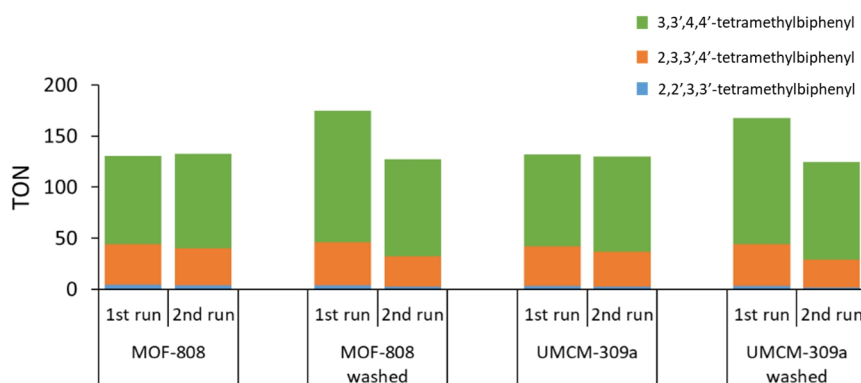


Figure S1. Effect of an extra washing step with a 0.1 M aqueous solution of sodium acetate on the TON of the oxidative coupling of *o*-xylene performed under the standard reaction conditions.

UMCM-309a

UMCM-309a was synthesized in a 250 mL pyrex Schott bottle by dissolving 0.117 g (0.50 mmol) zirconium(IV) chloride (Sublimed 99.95 % Zr, ABCR) and 0.110 g (0.25 mmol) 1,3,5-tris(4-carboxyphenyl)benzene (homemade linker)⁶ in 45 mL DMF (>99 %, Acros). Subsequently, 11 mL formic acid (98 %, Carl Roth), 5 mL hydrochloric acid (37 % solution in water, Fisher) and 5 mL methanol (HPLC grade, Acros) were added. The resulting solution was then placed in a synthesis oven at 100 °C for 18 h.

After synthesis, the obtained precipitate was washed two times with DMF, three times with methanol and dried at 180 °C for 8 h. To remove the chloride anions and modulators from the Zr-clusters, the same washing procedure as for MOF-808 was applied.

Zr-abtc

Zr-abtc was synthesized according to a newly developed green synthesis procedure in water. In a 100 mL round bottom flask, 0.891 g (2.76 mmol) zirconyl chloride octahydrate (>98 %, ABCR) and 0.895 g (2.50 mmol) 3,3',5,5'-azobenzene-tetracarboxylate (h_4 abtc) were mixed with 25 ml formic acid (97 %, Alfa Aesar) and 25 ml water and the resulting mixture was heated under reflux for three hours. After synthesis, the obtained precipitate was washed with ethanol and dried at 115 °C under vacuum (1 mbar) for 24 hours.

The h_4 abtc linker was synthesized according a literature procedure.⁷

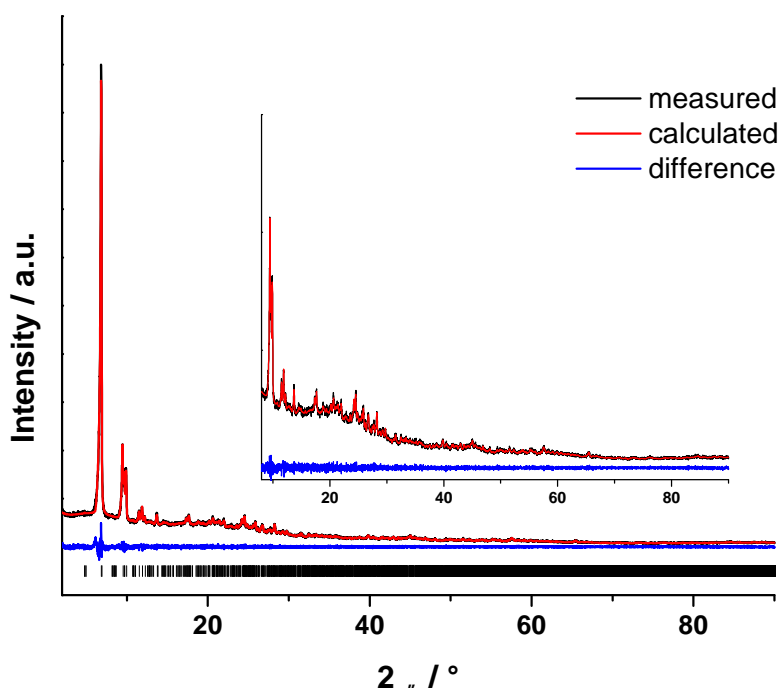


Figure S2. Le-Bail fit of Zr-abtc synthesized following the newly developed green synthesis procedure.

The cell parameters of Zr-abtc synthesized following our newly developed green synthesis procedure match with the values described in the literature.⁸

Compound	Zr-abtc (literature)	Zr-abtc (green synthesis procedure)
Space Group	<i>C2/m</i>	<i>C2/m</i>
Crystal System	Monoclinic	Monoclinic
a / Å	25.4692(11)	25.5(1)
b / Å	36.3589(15)	36.3(1)
c / Å	21.5275(9)	21.61(9)
α / °	90	90
β / °	122.260(2)	122.57(2)
γ / °	90	90
Rwp	---	4.5
GoF	---	1.6

UiO-66-COOH

UiO-66-BDC-COOH was prepared by following a green synthesis route.⁹ First, 190 g (0.53 mol) $\text{Zr}(\text{SO}_4)_2 \cdot 4\text{H}_2\text{O}$ was dissolved in 2.70 L deionized water under stirring. Once a clear solution was obtained, 449 g (0.124 mol) of 1,2,4-benzenetricarboxylic acid was added and the mixture was refluxed for 4 h at 97 °C. The resulting slurry was filtrated while still warm and washed with deionized water and ethanol. Finally, the obtained powder was dried at 100 °C.

UiO-66

UiO-66 was synthesized in a 1 L pyrex Schott bottle by dissolving 3.360 g (20.00 mmol) terephthalic acid (99+ %, Acros), 3.105 g (13.30 mmol) zirconium(IV) chloride (Sublimed 99.95 % Zr, ABCR) and 2 mL hydrochloric acid (37 % solution in water, Fisher) in 400 mL DMF (>99 %, Acros). The resulting solution was then placed in a synthesis oven at 120 °C for 24 h.

After synthesis, the obtained precipitate was washed three times with DMF, three times with ethanol and dried at 115 °C under vacuum (1 mbar) for 24 hours. In each step, the material was centrifuged at 4000 rpm for 20 min and the supernatant was decanted.

UiO-67-bipy

UiO-67 was synthesized in a 250 mL pyrex Schott bottle by dissolving 0.310 g (1.27 mmol) 2,2'-bipyridine-5,5'-dicarboxylic acid (97 %, Sigma-Aldrich) in 100 mL *N,N*-dimethylformamide (DMF) (>99 %, Acros). After sonication, 0.296 g (1.27 mmol) zirconium(IV) chloride (99 %, ABCR) was added, followed by 2 mL acetic acid (glacial, Fisher) and 0.5 mL hydrochloric acid (37 % solution in water, Fisher). The resulting solution was then placed in a synthesis oven at 120 °C for 48 h.

After synthesis, the obtained precipitate was washed three times with DMF and three times with ethanol. In each step, the material was centrifuged at 4000 rpm for 20 min and the supernatant was decanted. After the washing steps, the material was dried at 115 °C under vacuum (1 mbar) for 24 hours.

Zirconium oxide

Zirconium oxide was purchased from Alfa Aesar and used after drying at 115 °C under vacuum (1 mbar) for 24 hours.

Smopex-102

Smopex-102 is a commercially available acrylic acid grafted polyolefin fiber of Johnson Matthey. The cation exchange capacity of this polymer with pendent carboxylic acid groups is 7-10 mmol/g.

MOF loading

Table S1. Pd loading of the different MOFs under the standard reaction conditions. ^aTheoretical percentage of anchoring sites occupied by Pd based on the structure formulas of the MOFs. ^bOptimized reaction conditions.

entry	MOF support	type of anchoring site	anchoring sites occupied by Pd (%) ^a
1	UiO-67-bipy	bipyridine moiety	17
2	UiO-66-COOH	pendent carboxylic acid group	17
3	MOF-808	OH/OH ₂ pair on Zr-cluster	17
4	UMCM-309a	OH/OH ₂ pair on Zr-cluster	17
5	Zr-abtc	OH/OH ₂ pair on Zr-cluster	25
6	UiO-66	/	/
7	Smopex-102	pendent carboxylic acid group	17
8 ^b	MOF-808	OH/OH ₂ pair on Zr-cluster	3

The MOF supports were usually loaded *in situ* with Pd(OAc)₂, although preloading in *o*-xylene or heptane could also be achieved. Generally, 8.23 mg (36.66 μmol) Pd(OAc)₂ was added to 50.00 mg (36.66 μmol) MOF-808 in 1 mL *o*-xylene or heptane, implying that only 1 out of maximally 6 anchoring sites is occupied by Pd. After stirring this slurry overnight, the solvent became colorless and was removed after centrifugation. The palladium loaded MOF powders were then dried under vacuum (1 mbar) at room temperature. The mass of the preloaded samples after drying was 58.06 mg and 58.18 mg for preloading in heptane and *o*-xylene, respectively, confirming that the solvent was efficiently removed.

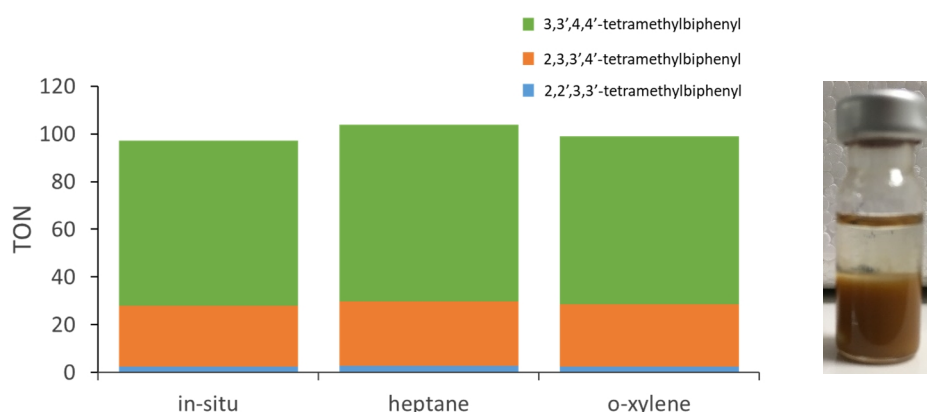


Figure S3. Left: comparison of in situ loaded and preloaded MOF-808 supports for the oxidative coupling of *o*-xylene performed under the standard reaction conditions. Right: picture of Pd loaded MOF-808 after preloading in *o*-xylene overnight.

Optimization of the reaction conditions

Table S2. Optimization of the reaction conditions^a

entry	MOF support	strongly acidic additive	co-solvent	temperature (°C)	chemo-selectivity (%) ^b	regio-selectivity (%) ^c	yield (%) ^d	TON ^e
1	<i>f</i>	1-PrSO₃H	acetic acid	90	89	53	0.1	97
2 ^g	/	1-PrSO ₃ H	acetic acid	90	no biaryl products detected			
3	/	p-TsOH	acetic acid	90	91	69	4.1	81
4	/	BSO ₃ H	acetic acid	90	93	64	3.4	68
5	/	MeSO ₃ H	acetic acid	90	90	61	1.6	32
6	/	Bi(OTf) ₃ ^h	acetic acid	90	92	45	3.0	59
7	/	1-PrSO ₃ H	benzoic acid	90	90	73	4.7	93
8	/	1-PrSO ₃ H	pivalic acid	90	88	74	4.6	92
9	UiO-67-bipy	1-PrSO ₃ H	acetic acid	90	74	66	0.3	6
10	4,4'-dimethyl-2,2'-bipyridine ⁱ	1-PrSO ₃ H	acetic acid	90	51	83	0.1	1
11	UiO-66-COOH	1-PrSO ₃ H	acetic acid	90	92	73	7.4	149
12	MOF-808	1-PrSO₃H	acetic acid	90	92	74	9.2	183
13	UMCM-309a	1-PrSO ₃ H	acetic acid	90	93	74	8.4	168
14	Zr-abtc	1-PrSO ₃ H	acetic acid	90	93	73	7.1	142
15	UiO-66	1-PrSO ₃ H	acetic acid	90	90	75	5.2	103
16	MOF-808	1-PrSO ₃ H	acetic acid ^j	90	86	73	5.4	107

17	MOF-808	1-PrSO ₃ H	acetic acid ^k	90	92	70	7.9	158
18	MOF-808	1-PrSO ₃ H	acetic acid ^l	90	91	66	5.2	104
19	MOF-808	1-PrSO ₃ H ^m	acetic acid	90	89	73	2.9	57
20	MOF-808	1-PrSO ₃ H ⁿ	acetic acid	90	92	72	6.9	138
21	MOF-808 ^o	1-PrSO ₃ H	acetic acid	90	89	57	0.2	4
22	MOF-808 ^o	1-PrSO ₃ H ^p	acetic acid	90	91	73	5.6	111
23	MOF-808 ^o	1-PrSO ₃ H ^q	acetic acid	90	91	73	6.6	133
24	MOF-808 ^o	1-PrSO ₃ H ^r	acetic acid	90	89	71	6.1	121
25	MOF-808	1-PrSO ₃ H	acetic acid	25	89	53	0.1	1
26	MOF-808	1-PrSO₃H	acetic acid	110	94	75	21.9	437
27	MOF-808	1-PrSO ₃ H	acetic acid	130	91	64	19.7	395
28	MOF-808	1-PrSO ₃ H	acetic acid	150	91	58	17.8	356
29	MOF-808	1-PrSO ₃ H	acetic acid	170	89	46	10.9	219
30^s	MOF-808^o	1-PrSO₃H^q	acetic acid	110	94	75	21.8	436
31 ^t	MOF-808 ^o	1-PrSO ₃ H ^q	acetic acid	110	90	74	13.8	276

^aStandard reaction conditions: *o*-xylene (16.58 mmol), Pd(OAc)₂ (8.29 μmol; 0.05 mol %), MOF support (8.29 μmol; 0.05 mol %), strongly acidic additive (82.85 μmol; 0.5 mol %), co-solvent (2.07 mmol; 12.5 mol %), 90 °C, 16 bar O₂, 17 h. ^bChemoselectivity is defined as the percentage of biaryls relative to all formed products (oxidation products, biaryls and triaryls). ^cRegioselectivity is defined as the percentage of 3,3',4,4'-tetramethylbiphenyl relative to all three biaryls. ^dYield was determined by GC-FID with hexadecane as internal standard. ^eTON is defined as TON = 2 x mole (biaryl) / mole (Pd). ^fHomogeneous reaction without MOF support. ^gControl experiment without Pd(OAc)₂. ^h4.14 μmol (0.025 mol %) Bi(OTf)₃. ⁱ8.29 μmol (0.05 mol %) 4,4'-dimethyl-2,2'-bipyridine was added to mimic the conditions of entry 8 with UiO-67-bipy. ^j16.58 mmol (100 mol %) acetic acid. ^k0.83 mmol (5 mol %) acetic acid. ^l0.41 mmol (2.5 mol %) acetic acid. ^m41.43 μmol (0.25 mol %) 1-propanesulfonic acid.

^a124.28 μmol (0.75 mol %) 1-propanesulfonic acid. ^b41.43 μmol (0.25 mol %) MOF-808. ^c289.98 μmol (1.75 mol %) 1-propanesulfonic acid. ^d331.40 μmol (2.00 mol %) 1-propanesulfonic acid. ^e372.83 μmol (2.25 mol %) 1-propanesulfonic acid. ^fAverage of three measurements. ^g1.81 mmol (10.90 mol %) H₂O added to the reaction mixture (approximately the amount of water formed in entry 30 during the reaction) to show the deactivation effect of *in situ* formed water.

Palladium leaching

Table S3. Effect of the MOF supports on the amount of Pd leaching in the reaction solution after reaction performed under the standard reaction conditions. The values were determined by ICP-OES. Zr leaching was found to be < 0.5 %, indicating that these MOFs are stable under the standard reaction conditions. For the homogeneous reaction, 98 % of the added Pd content was found which validates the experimental method.

entry	MOF support	leaching (ppm)	leaching (%)
1	/	437	98
2	MOF-808	21	5
3	UMCM-309a	40	9
4	Zr-abtc	26	6
5	UiO-66-COOH	36	8
6	UiO-66	64	14
7	Smopex-102	32	7

Table S4. The amount of Pd leaching in the reaction solution after reaction performed under the optimized reaction conditions and with reactivation of the Pd loaded MOF. The values were determined by ICP-OES and are the average of three experiments. Zr leaching was found to be <0.1 %.

entry	run	leaching (ppm)	leaching (%)
1	1 st	10 \pm 2.3	2 \pm 0.5
2	2 nd	9 \pm 0.4	2 \pm 0.1
3	3 rd	4 \pm 0.7	1 \pm 0.1
Total		23 \pm 2.5	5 \pm 0.5

Hot filtration test

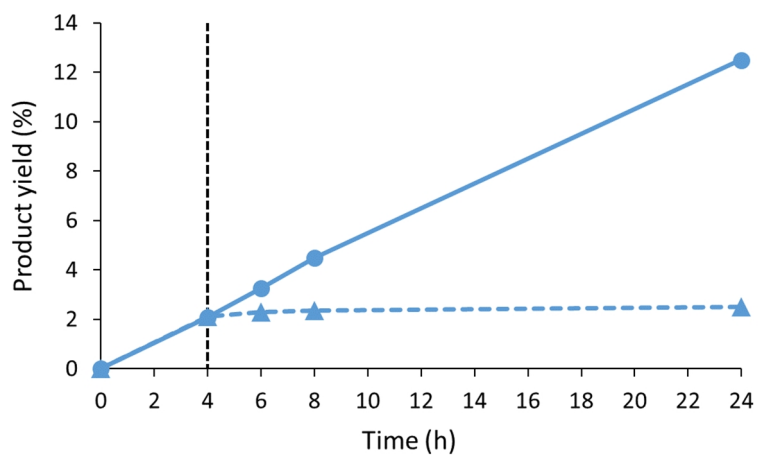


Figure S4. Hot filtration test of the oxidative coupling of *o*-xylene with MOF-808 under the standard reaction conditions. The reaction solution was filtered after 4 hours (vertical dashed line). While the yield of the retentate (solid line) increases significantly, the yield of the filtrate (dashed line) does not increase distinctly, indicating that the reaction occurs heterogeneously within the pores of the MOF-support.

PXRD

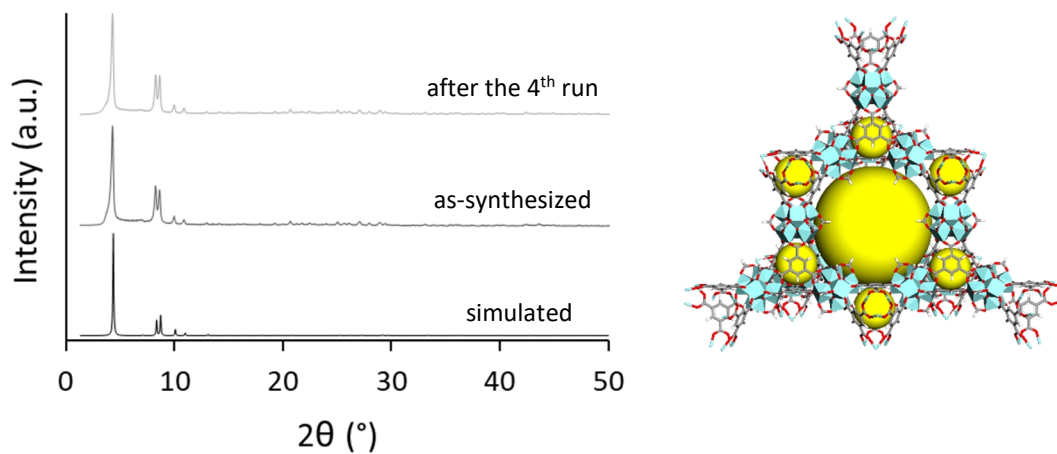


Figure S5. PXRD patterns (simulated, as-synthesized and after the 4th run performed under the standard conditions) of MOF-808 (left) and a structural model of MOF-808 (right).

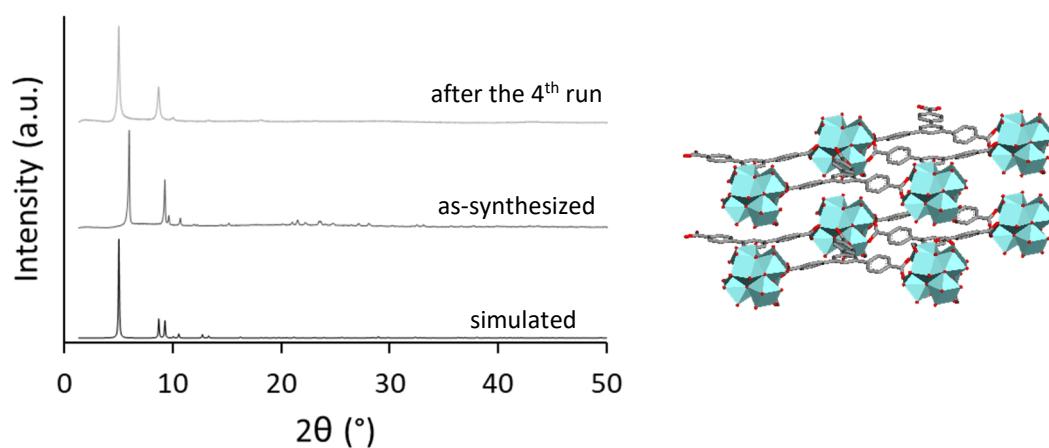


Figure S6. PXRD patterns (simulated, as-synthesized and after the 4th run performed under the standard conditions) of UMCM-309a (left) and a structural model of UMCM-309a (right). The reflections are slightly shifted due to differences in the interlayer distance between the two-dimensional layers.

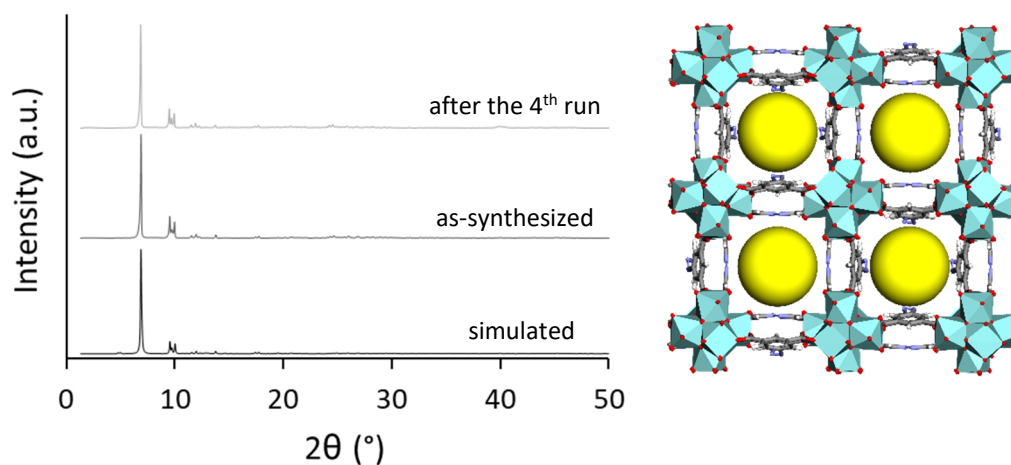


Figure S7. PXRD patterns (simulated, as-synthesized and after the 4th run performed under the standard conditions) of Zr-abtc (left) and a structural model of Zr-abtc (right).

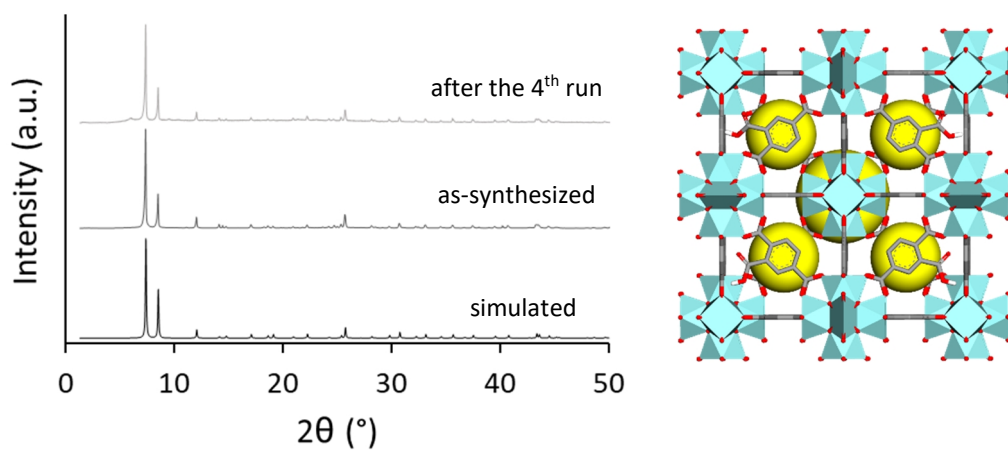


Figure S8. PXRD patterns (simulated, as-synthesized and after the 4th run performed under the standard conditions) of UiO-66-COOH (left) and a structural model of UiO-66-COOH (right).

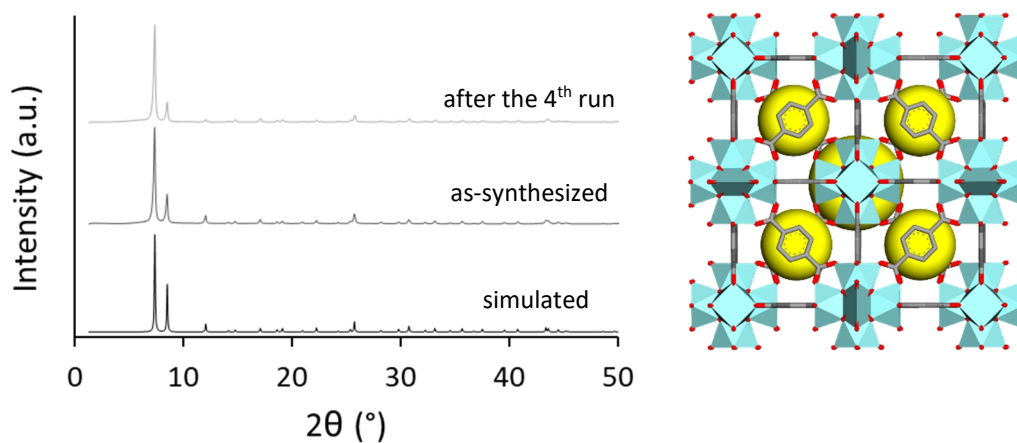


Figure S9. PXRD patterns (simulated, as-synthesized and after the 4th run performed under the standard conditions) of UiO-66 (left) and a structural model of UiO-66 (right).

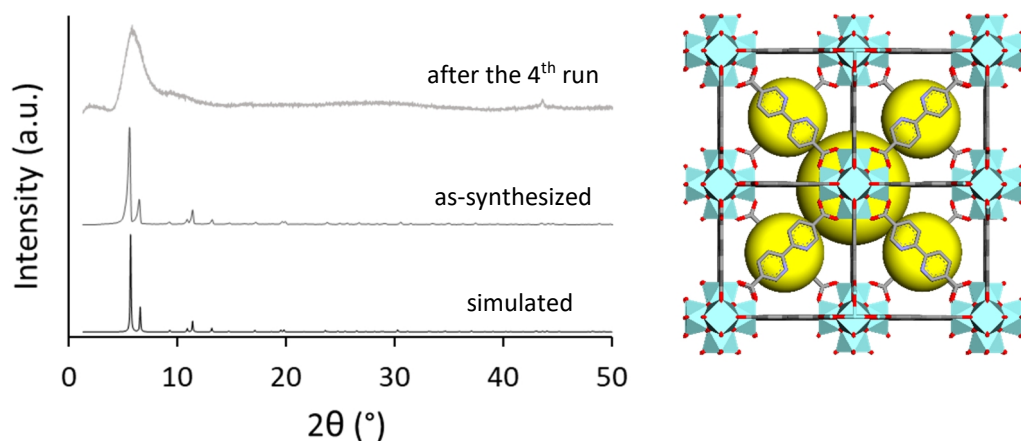


Figure S10. PXRD patterns (simulated, as-synthesized and after the 1st run performed under the standard conditions) of UiO-67-bipy (left) and a structural model of UiO-67-bipy (right).

Substrate scope

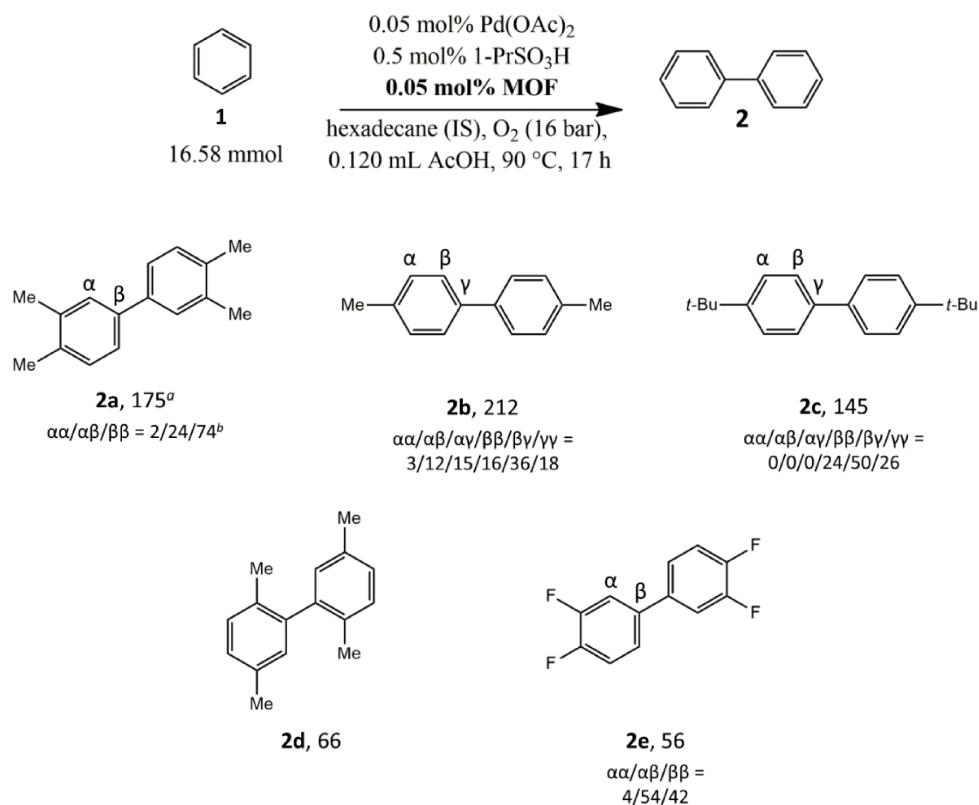


Figure S11. Oxidative coupling of simple arenes (*o*-xylene; **2a**, toluene; **2b**, *tert*-butylbenzene; **2c**, *p*-xylene; **2d** and 1,2-difluorobenzene; **2e**) performed under the standard reaction conditions. The values under each structure indicate TONs^a and regioisomers (%)^b.

MOF stability

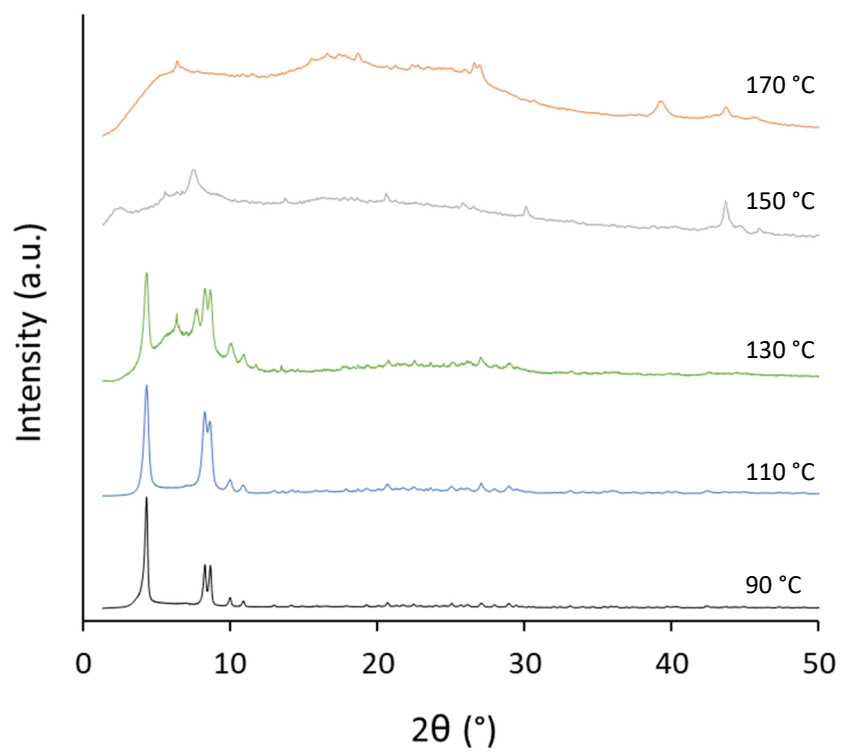


Figure S12. Effect of reaction temperature on the crystallinity of MOF-808.

Product inhibition experiments

Product inhibition experiments were performed on the homogeneous reaction by adding water and bixylyl product to distinguish between product inhibition and catalyst deactivation. The initial amount of *o*-xylene of the reactions in entry 2, 3 and 4 (16.21 mmol) equals the amount of *o*-xylene of the reaction under the standard reaction conditions in entry 1 after 6 h (when 2.25 % of the original 16.58 mmol has been converted) (Table S5). Furthermore, 0.19 mmol water or bixylyl product (3,3',5,5'-tetramethylbiphenyl) were added to the reactions of entries 3 and 4, respectively. This is the same amount of water and bixylyl products formed *in situ* in the reaction of entry 1 after 6 h.

Table S5. Reaction conditions of the product inhibition experiments performed under the standard reaction conditions. ^a3,3',5,5'-tetramethylbiphenyl was used as bixylyl product.

entry	<i>o</i> -xylene (mmol)	water (mmol)	bixylyl product (mmol) ^a
1	16.58	0	0
2	16.21	0	0
3	16.21	0.19	0
4	16.21	0	0.19

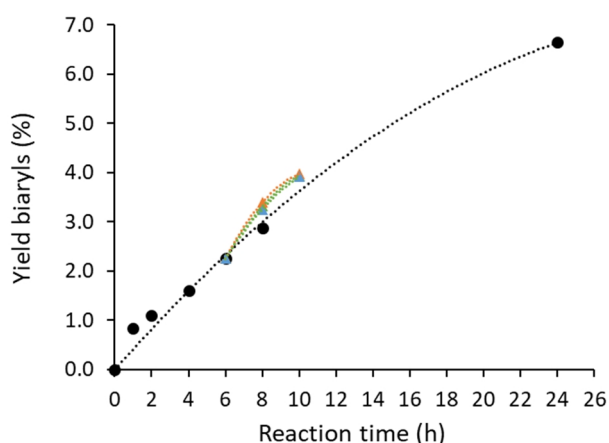


Figure S13. Time-adjusted kinetic profiles of the oxidative coupling of *o*-xylene performed under the standard reaction conditions without MOF support: black (Table S5, entry 1), blue (Table S5, entry 2), orange (Table S5, entry 3), green (Table S5, entry 4). Lines were added as a guide to the eye.

The time-adjusted kinetic profiles of the reactions of entries 2, 3 and 4 are almost identical but do not match the profile of entry 1 (Figure S13). Hence, this implies that the decrease in yield over time is predominantly due to catalyst deactivation and not inhibition by the added products like water or bixylyl. This also confirms our hypothesis that isolation of the active sites on the MOF supports prolongs catalyst lifetime, since the decrease in yield over time is less pronounced when MOF supports are added (Figure 5). However, after many catalytic cycles (TONs > 400), a large amount of water is formed and product inhibition due to water formation is observed (see Table S2, entries 30 and 31). For instance, when 1.81 mmol water is added, only 276 TONs can be achieved after 17 h under the optimized reaction conditions instead of 436. Drying of the MOF supports after each run under vacuum at room temperature for 24 h solves this issue (Figure S14).

Catalyst reactivation

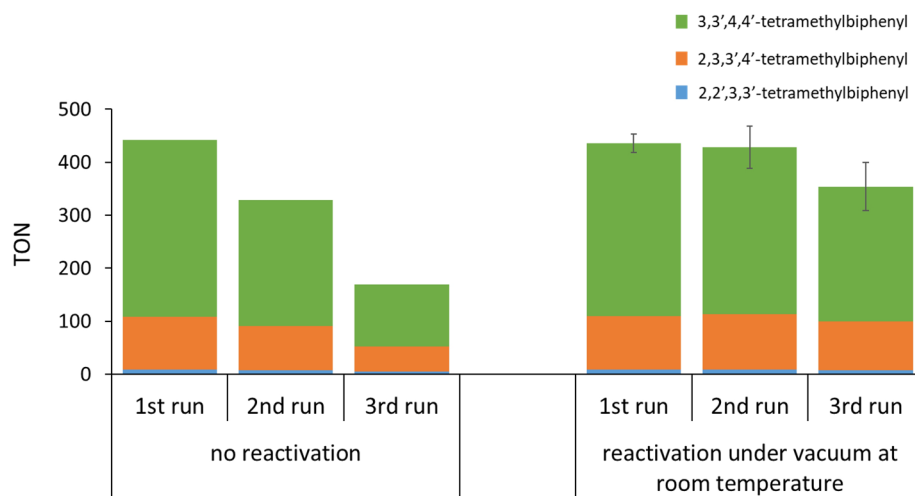


Figure S14. Effect of reactivation under vacuum (1 mbar) at room temperature for 24 h on the TON of the oxidative coupling of *o*-xylene performed under optimized reaction conditions. Conditions: *o*-xylene (16.58 mmol), Pd(OAc)₂ (8.29 μmol; 0.05 mol %), MOF support (41.43 μmol; 0.25 mol %), strongly acidic additive (331.40 μmol; 2.00 mol %), co-solvent (2.07 mmol; 12.5 mol %), 110 °C, 20 bar O₂, 17 h.

FTIR

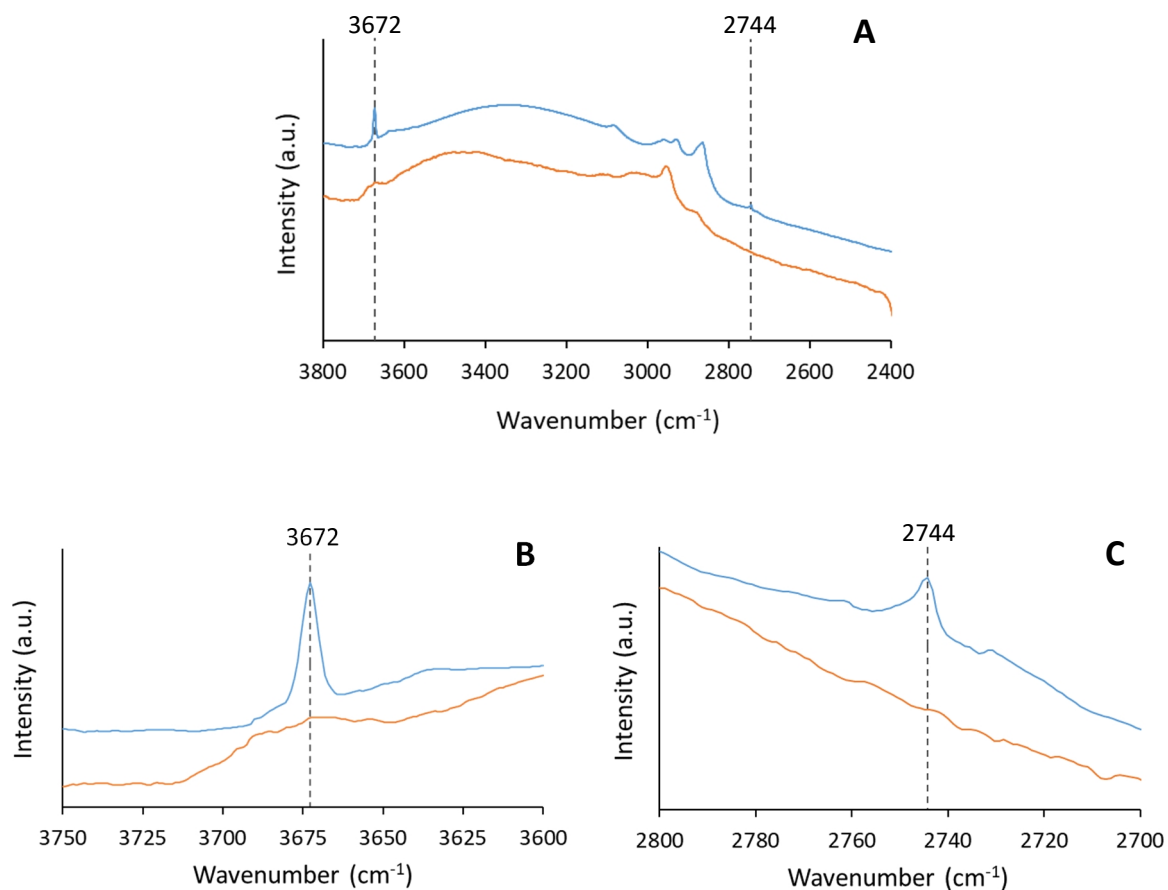


Figure S15. IR spectrum (A) of bare MOF-808 (blue) and preloaded MOF-808 (6 Pd per Zr-cluster) (orange). Zoomed-in spectra of the IR bands of non-hydrogen-bonded OH groups and μ_3 -OH groups (3672 cm⁻¹) (B) and hydrogen-bonded OH/OH₂ pairs (2744 cm⁻¹) (C). The spectra are shifted vertically for clarity.

EXAFS

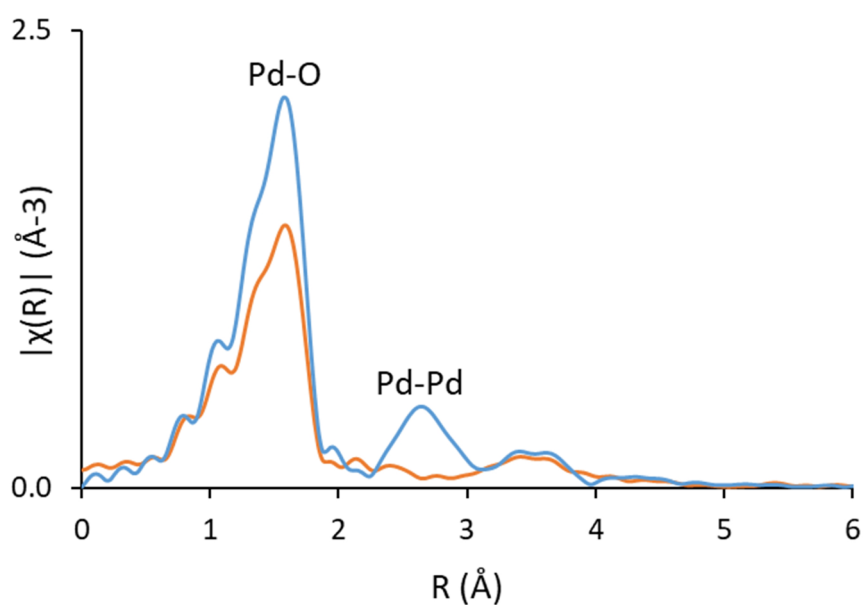
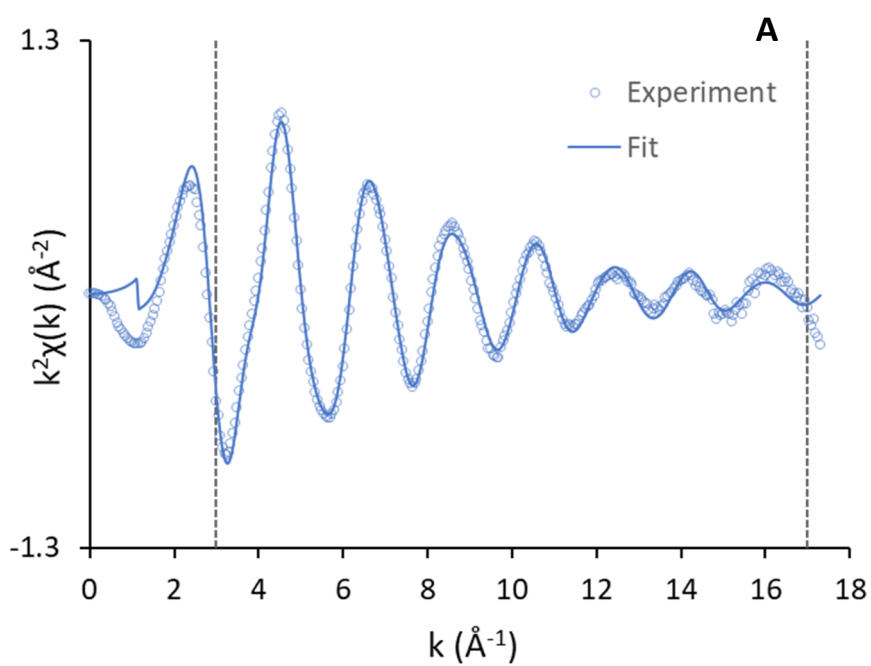


Figure S16. The magnitude of the Fourier transform of the experimental k^2 -weighted Pd k-edge EXAFS spectra of $\text{Pd}(\text{OAc})_2$ (blue) and preloaded MOF-808 (1 Pd per Zr-cluster in *o*-xylene) (orange) in R-space. The absence of a clear peak around 2.6 Å for preloaded MOF-808 confirms that the trimeric $\text{Pd}(\text{OAc})_2$ complexes are predominantly converted into monomeric, MOF-supported Pd(II) species.



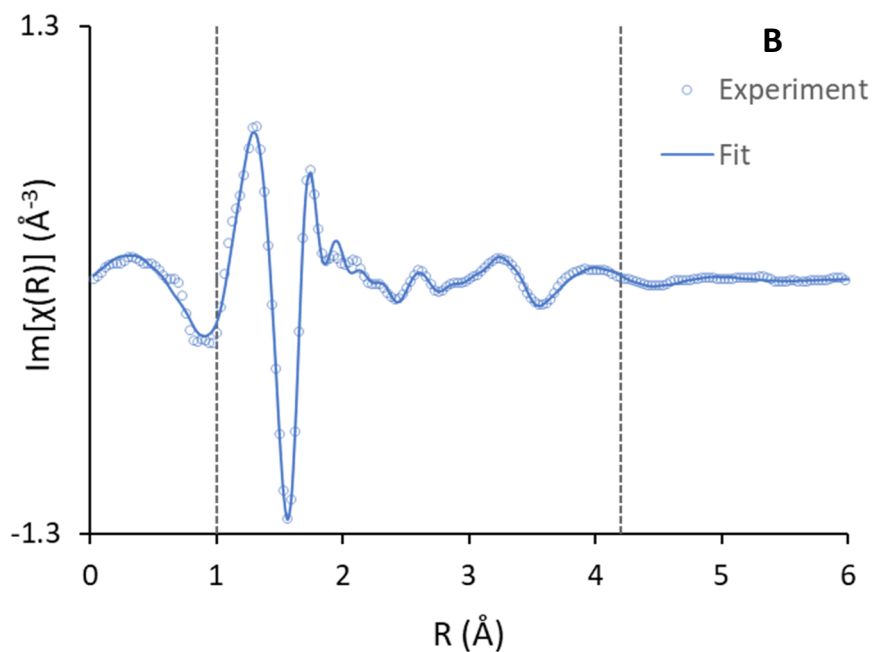


Figure S17. Experimental k^2 -weighted Pd k -edge EXAFS spectra of preloaded MOF-808 (1 Pd per Zr-cluster in *o*-xylene) (hollow circles) and the corresponding fits of the structure model (solid lines). $k^2\chi(k)$ plot (A) and the imaginary component of the Fourier transform of the EXAFS data (B). The vertical dashed lines indicate the fitting ranges.

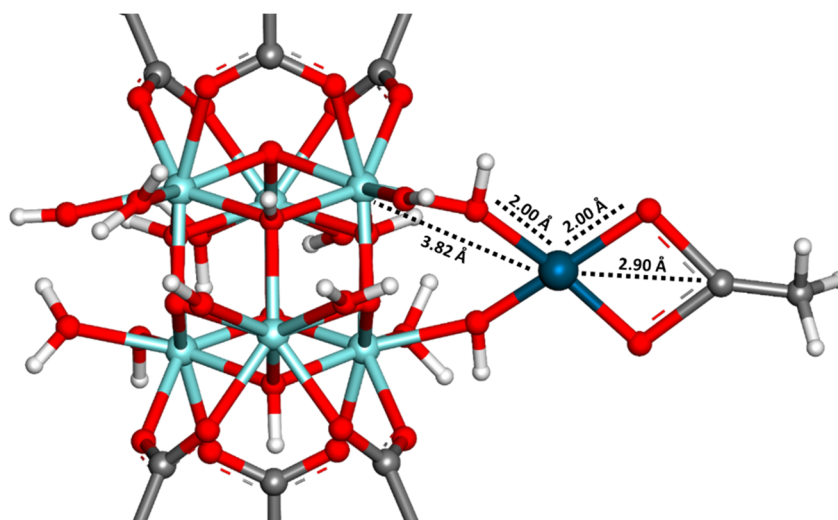


Figure S18. Schematic representation of the fitted structure model of Pd(II) anchored on the Zr-cluster of MOF-808

Table S6. Best-fit EXAFS parameters of the fitted Pd K-edge EXAFS spectrum of preloaded MOF-808 (1 Pd per Zr-cluster in *o*-xylene)

shell	N	R (Å)	$10^3 \times \Delta\sigma^2$ (Å ²)	ΔE_0 (eV)	R (%)	1.24
Pd–O _{Ac}	2.05 ± 0.22	2.00 ± 0.02	2.2 ± 1.0	-5.1 ± 1.7	χ^2_{ν}	388
Pd–O _{Zr}	2.02 ± 0.22	2.00 ± 0.03	5.5 ± 3.8	4.8 ± 2.3	ΔR (Å)	[1.0 - 4.2]
Pd–C _{Ac}	1.02 ± 0.11	2.90 ± 0.03	2.4 ± 2.8	-5.1 ± 1.7	Δk (Å ⁻¹)	[3.0 - 17.0]
Pd–Pd	/	/	/	/	N_{ipd}	28
Pd–Zr	2.02 ± 0.22	3.82 ± 0.10	14.1 ± 7.6	-13.0 ± 9.1	N_{var}	18

High-angle annular dark-field scanning transmission electron microscopy (HAADF-STEM)

High-angle annular dark-field scanning transmission electron microscopy (HAADF-STEM) in combination with energy-dispersive X-ray spectroscopy (EDX) was used to analyze preloaded MOF-808 and MOF-808 after reaction. A sample of UiO-66 after reaction was also analyzed for comparison since this MOF does not contain anchoring sites. Although Pd nanoparticles can be observed on MOF-808 after reaction (Figure S20, A), these nanoparticles are homogeneously dispersed over the MOF with a narrow size distribution (Figure S20, C). No clear Pd nanoparticles aggregation is visible (Figure S22, B). In contrast, Pd nanoparticle aggregation can clearly be observed in UiO-66 after reaction and the Pd nanoparticles are up to 100 nm in size (Figure S21, A and Figure S22, C). This indicates that palladium anchoring on the Zr-clusters of MOF-808 reduces Pd nanoparticle aggregation.

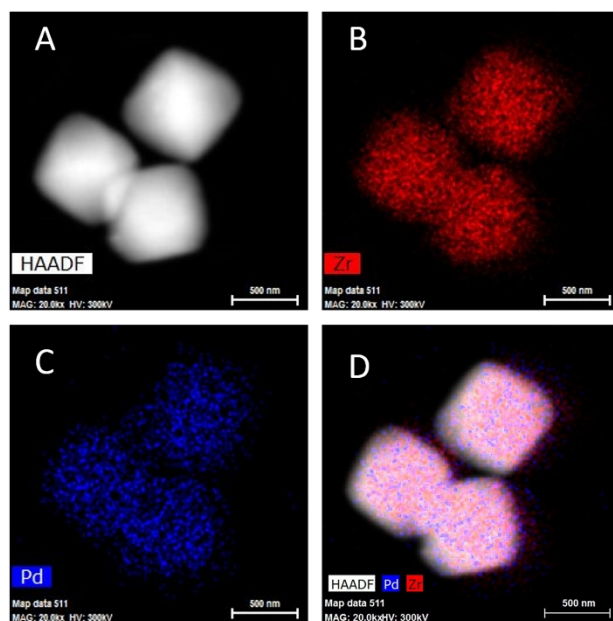


Figure S19. High-angle annular dark-field scanning transmission electron microscopy (HAADF-STEM) images of preloaded MOF-808 (A) in combination with energy-dispersive X-ray spectroscopy (EDX) displaying Zr mapping in red (B), palladium mapping in blue (C) and an overlay of both (D). No obvious Pd nanoparticles can be observed.

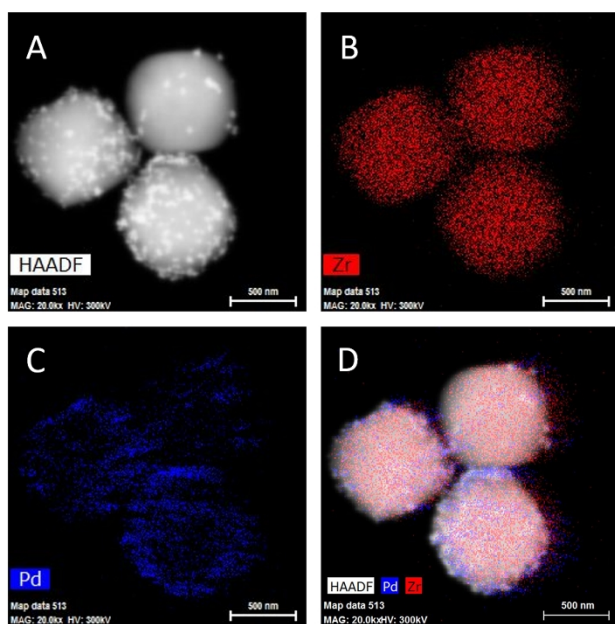


Figure S20. High-angle annular dark-field scanning transmission electron microscopy (HAADF-STEM) images of MOF-808 after reaction under the standard reaction conditions (A) in combination with energy-dispersive X-ray spectroscopy (EDX) displaying Zr mapping in red (B), palladium mapping in blue (C) and an overlay of both (D). Although Pd nanoparticles can be seen in MOF-808 after reaction (A), they are relatively small and well distributed over the MOF particles (C). No clear Pd nanoparticle aggregation is visible. The size of the Pd nanoparticles is limited to 30 nm.

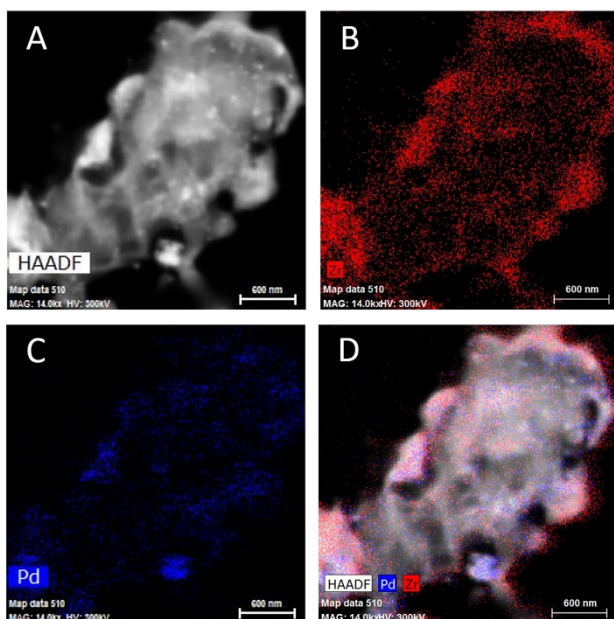


Figure S21. High-angle annular dark-field scanning transmission electron microscopy (HAADF-STEM) images of UiO-66 after reaction under the standard reaction conditions (A) in combination with energy-dispersive X-ray spectroscopy (EDX) displaying Zr mapping in red (B), palladium mapping in blue (C) and an overlay of both (D). Pd nanoparticle aggregation can clearly be observed (A and C) and the Pd nanoparticles are up to 100 nm in size.

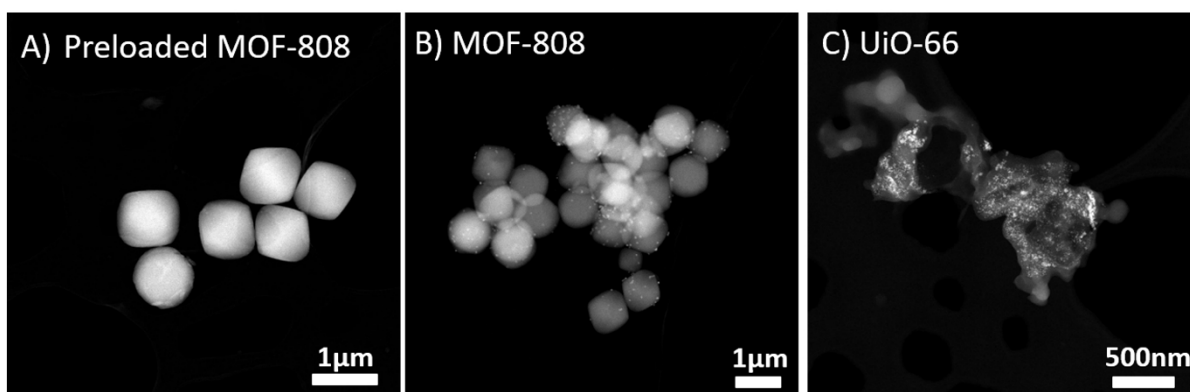


Figure S22. High-angle annular dark-field scanning transmission electron microscopy (HAADF-STEM) images of (A) preloaded MOF-808; no Pd nanoparticles are observed, (B) MOF-808 after reaction; Pd nanoparticles are observed and found to be homogeneously dispersed on the MOF crystals within a narrow size distribution and (C) UiO-66 after reaction; Pd nanoparticle aggregation can clearly be observed.

Influence of the oxygen pressure

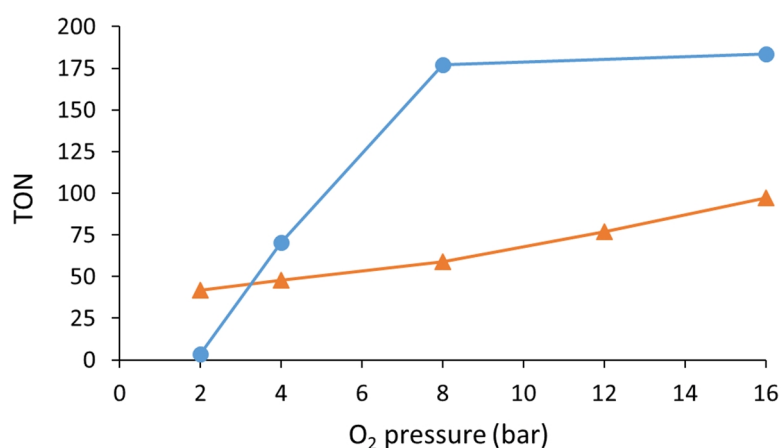


Figure S23. Influence of O₂ pressure on the TON of the oxidative coupling of *o*-xylene under the standard reaction conditions for the homogeneous reaction (orange) and the reaction with MOF-808 (blue). The plateau at > 8 bar for the reaction with MOF-808 indicates that there are no deactivation issues under these conditions.

Determination of the Kinetic Isotope Effect

The general procedure for the catalytic reactions was slightly adapted to determine the Kinetic Isotope Effect. Briefly, 2.000 mL (16.58 mmol) *o*-xylene or 2.022 mL (16.58 mmol) *o*-xylene-d₁₀ (Sigma, 99 %, 99 atom % D), 8.30 μL (82.85 μmol) 1-propanesulfonic acid, 0.118 mL (2.07 mmol) acetic acid and 0.1 mL hexadecane (internal standard) were added to 1.86 mg (8.29 μmol) Pd(OAc)₂ and (8.29 μmol) MOF in a 10 mL stainless steel autoclave. The oxygen pressure was set to 16 bar and the reaction was conducted under stirring at 90 °C for 1.5 hours in a preheated 4-well aluminum block. After reaction, the reactors were cooled on ice, the MOF was separated from the reaction medium via centrifugation and the products were analyzed using GC-FID/GC-MS.

References

- 1 S. Nikitenko, A. M. Beale, A. M. J. Van Der Eerden, S. D. M. Jacques, O. Leynaud, M. G. O'Brien, D. Detollenaere, R. Kaptein, B. M. Weckhuysen and W. Bras, *J. Synchrotron Radiat.*, 2008, **15**, 632–640.
- 2 B. Ravel and M. Newville, *J. Synchrotron Radiat.*, 2005, **12**, 537–541.
- 3 Y. Izawa and S. S. Stahl, *Adv. Synth. Catal.*, 2010, **352**, 3223–3229.
- 4 D. Wang and S. S. Stahl, *J. Am. Chem. Soc.*, 2017, **139**, 5704–5707.
- 5 T. C. Wang, N. A. Vermeulen, I. S. Kim, A. B. F. Martinson, J. Fraser Stoddart, J. T. Hupp and O. K. Farha, *Nat. Protoc.*, 2016, **11**, 149–162.
- 6 J. Kim, B. Chen, T. M. Reineke, H. Li, M. Eddaoudi, D. B. Moler, M. O. Keeffe and O. M. Yaghi, 2001, **123**, 8239–8247.
- 7 S. Ameerunisha and P. S. Zacharias, *J. CHEM. SOC. PERKIN TRANS.*, 1995, **2**, 1679–1682.
- 8 H. Wang, X. Dong, J. Lin, S. J. Teat, S. Jensen, J. Cure, E. V. Alexandrov, Q. Xia, K. Tan, Q. Wang, D. H. Olson, D. M. Proserpio, Y. J. Chabal, T. Thonhauser, J. Sun, Y. Han and J. Li, *Nat. Commun.*, 2018, **9**, 1–11.
- 9 H. Reinsch, D. Fröhlich, S. Waitschat, S. Chavan, K.-P. Lillerud, S. Henninger and N. Stock, *React. Chem. Eng.*, 2018, **3**, 365–370.